



spin magnetic moment, demonstrates the collapse of the short-range magnetic state under these conditions.

The final examples in the chapter involve crystal structure analysis via high-resolution-powder or single-crystal techniques, giving insight into the electronic behaviour and superconductivity in hole-doped $\text{Nd}_{1-x}\text{Sr}_x\text{FeAsO}$; the solution of the crystal structure of novel organometallic complexes of copper with peptides, which reveals a pleasing network of hydrogen bonds; and metal-organic framework materials containing rare-earth ions that combine high thermal stability and other multifunctional properties (magnetism, luminescence, microporosity, hydrophobicity). The combination of a luminescent Ln^{3+} centre and the chosen ligands results in

materials that can sense ethanol in air even in the presence of water.

Preparations are underway for the experiments that will yield the articles of future editions of the ESRF highlights. Ideas and plans for improved experimental approaches are always being sought, and, with the start of the ESRF Upgrade Programme, two beamlines relevant to this chapter are under consideration. The first is for high-energy diffraction using a microfocussed beam for penetrating through or into samples with high spatial resolution, and the second is a fully-dedicated beamline for pump-probe time-resolved diffraction. These would each greatly enhance the ESRF's capabilities in these exciting areas.

A. Fitch

Principal publication and authors

Q. Kong (b), J.H. Lee (a),
A. Plech (c), M. Wulff (b),
H. Ihee (a), M.H.J. Koch (d),
Angew. Chem. Int. Ed. **47**, 5550
(2008).

(a) Center for Time-Resolved
Diffraction, Department of
Chemistry, KAIST, Daejeon
(Republic of Korea)

(b) ESRF

(c) Fachbereich Physik der
Universität Konstanz (Germany)

(d) EMBL, Hamburg Outstation
(Germany)

■ Ultrafast X-ray solution scattering reveals a new reaction intermediate in the photolysis of $\text{Ru}_3(\text{CO})_{12}$

The triangular metal carbonyl cluster $\text{Ru}_3(\text{CO})_{12}$ is one of the simplest thermally-stable metal carbonyls. The complex is used in controlled photoactivated synthesis where specific bonds in the complex are broken upon irradiation at different wavelengths. As the mechanism leading to the cleavage of metal-metal bonds is of great theoretical and practical interest, the photolysis of $\text{Ru}_3(\text{CO})_{12}$ has been extensively studied by spectroscopy in solid matrices and in solution. Structural characterisation of the intermediates has, however, been very difficult. Recent ultrafast infrared spectroscopy measurements have shown that when solutions of $\text{Ru}_3(\text{CO})_{12}$ in non-coordinating solvents like cyclohexane are excited with either an ultraviolet (266 nm) or a visible (400 nm) optical pulse, competing reactions yield two transient intermediates containing bridging carbonyls, $\text{Ru}_3(\text{CO})_{11}(\mu\text{-CO})$ (Intermediate 1) for the metal-metal

cleavage reaction channel and $\text{Ru}_3(\text{CO})_{10}(\mu\text{-CO})$ (Intermediate 2) for the CO loss reaction channel, respectively [1]. Infrared spectroscopy specifically monitors the time course of the concentration of these two intermediates via the characteristic absorption bands of their bridging carbonyls. This leaves the possibility that other intermediates could go unnoticed, especially those containing only terminal carbonyls with absorption bands overlapping those of the parent molecule.

In contrast to infrared spectroscopy, the signal from time-resolved X-ray or electron scattering contains contributions from all interatomic distances in the volume probed by the incident beam. In principle, this makes it possible to detect all transient intermediates [2]. Except for the simplest cases, however, there is no unique solution to recover the three-dimensional structural information

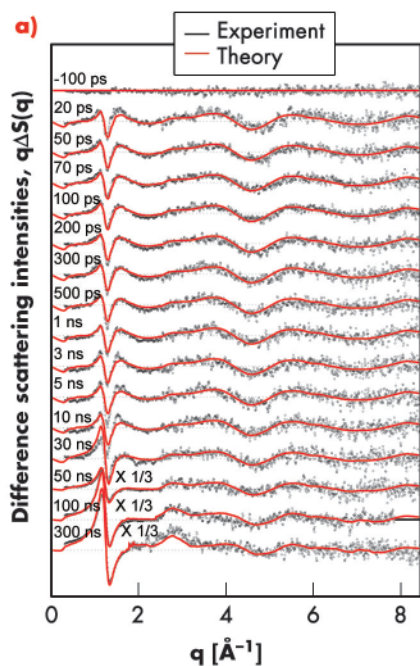
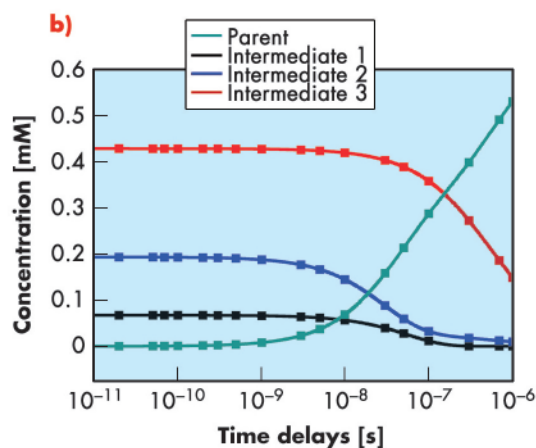


Fig. 21: a) Time-resolved difference scattering intensities $q\Delta S(q,t)$ as a function of time delays after photolysis of $\text{Ru}_3(\text{CO})_{12}$ in cyclohexane. The black dots correspond to the experimental data and the red curves to the theoretical least-squares fits. b) Concentration changes of the relevant chemical species during the photoreaction as a function of time.



from scattering data and this inverse problem can only be solved by modelling based on theoretical calculations. This approach was used to study the photodissociation of $\text{Ru}_3(\text{CO})_{12}$ dissolved in cyclohexane in a pump-probe experiment performed on beamline ID09B. Visible (390 nm) laser pulses (2 ps) were used for excitation and 100 picosecond X-ray pulses for probing the transient intermediates. In these experiments the sample flows through a nozzle which produces a thin layer of liquid. The pump-probe sequence is repeated with different time delays between pump and probe at a frequency of 986.3 Hz and the scattered signal is accumulated on a MarCCD detector. The difference X-ray scattering intensities ($q\Delta S(q,t)$) illustrating the structural changes due to the laser excitation are shown in **Figure 21a** as a function of different time delays.

Initial attempts at fitting the curves with only the known intermediates 1 and 2 failed to give satisfactory results and suggested the presence of a third intermediate. By modelling the measured difference scattering intensities $\Delta S(q,t)$ using the structures of 16 putative intermediates calculated by density functional theory (DFT), modelled in solution with molecular dynamics (MD) simulations, the concentration of each of the intermediates could be determined (**Figure 21b**). The results show that

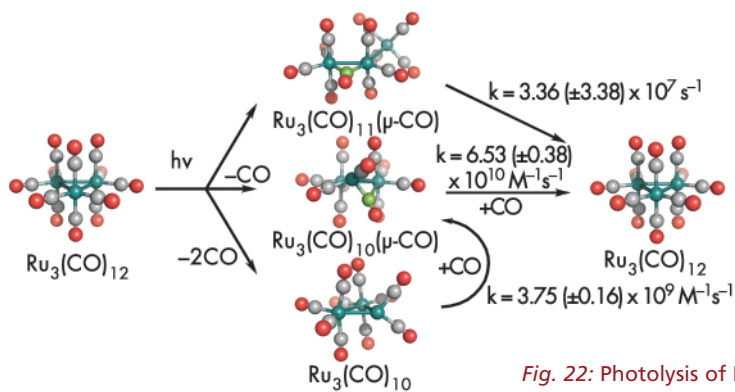


Fig. 22: Photolysis of $\text{Ru}_3(\text{CO})_{12}$ in cyclohexane probed in solution by time-resolved X-ray scattering. Beside the two known intermediates, $\text{Ru}_3(\text{CO})_{11}(\mu\text{-CO})$ and $\text{Ru}_3(\text{CO})_{10}(\mu\text{-CO})$, the hitherto undetected major intermediate $\text{Ru}_3(\text{CO})_{10}$ was found.

three intermediates, $\text{Ru}_3(\text{CO})_{11}(\mu\text{-CO})$, $\text{Ru}_3(\text{CO})_{10}(\mu\text{-CO})$ with bridged CO and $\text{Ru}_3(\text{CO})_{10}$ with terminal CO only, are formed at the onset of the reaction from the initial molecule $\text{Ru}_3(\text{CO})_{12}$, indicating the rupture of Ru-C and Ru-Ru bonds in $\text{Ru}_3(\text{CO})_{12}$ by the optical excitation. The new intermediate $\text{Ru}_3(\text{CO})_{10}$ with only terminal CO dominates at all time delays. It recombines non-geminately with one CO ligand to $\text{Ru}_3(\text{CO})_{10}(\mu\text{-CO})$ which eventually decays into the starting molecule $\text{Ru}_3(\text{CO})_{12}$ by non-geminate recombination with another CO. $\text{Ru}_3(\text{CO})_{11}(\mu\text{-CO})$ relaxes rapidly to the parent molecule $\text{Ru}_3(\text{CO})_{12}$ through geminate recombination.

These results strikingly illustrate the complementary nature of ultrafast X-ray scattering and ultrafast spectroscopy. Indeed, a good fit to the experimental X-ray scattering data could only be obtained if intermediate 3, which does not contain any bridging



References

- [1] E.A. Glascoe, M.F. Kling, J.E. Shanoski and C.B. Harris, *Organomet.* **25**, 775 (2006).
 [2] Q.Y. Kong, M. Wulff, J.H. Lee, S. Bratos and H. Ihee, *J. Am. Chem. Soc.* **129**, 13584 (2007).

Principal publication and authors

M. Di Vece (a), D. Grandjean (a), M.J. Van Bael (a), C.P. Romero (a), X. Wang (a), S. Decoster (b), A. Vantomme (b) and P. Lievens (a), *Phys. Rev. Lett.* **100**, 236105 (2008).

(a) *Laboratorium voor Vaste-
Stoffysica en Magnetisme &
INPAC - Institute for Nanoscale
Physics and Chemistry, K.U.
Leuven (Belgium)*

(b) *Instituut voor Kern- en
Stralingsfysica & INPAC - Institute
for Nanoscale Physics and
Chemistry, K.U. Leuven (Belgium)*

carbonyl and is thus invisible in infrared spectroscopy, is included in the refinement. It would have been very difficult using X-ray scattering alone to establish the existence of the minor intermediate $\text{Ru}_3(\text{CO})_{11}(\mu\text{-CO})$ because its contribution to the overall scattering curve is much smaller than

that of $\text{Ru}_3(\text{CO})_{10}$. As its existence has been unequivocally established by spectroscopy it is entirely justified to include it in the fit to the X-ray data. Together these techniques clearly indicate the existence of at least three intermediates with very different molecular structures (Figure 22).

Hydrogen-induced Ostwald ripening

The main aim in hydrogen storage research is to obtain high hydrogen concentrations in a material that possesses suitable transport properties under ambient conditions. A promising way to favourably alter the material's properties is by reducing its size to the extent that surface and quantum effects begin to play a major role. The investigation of nanocluster metal hydrides may therefore reveal novel properties. Palladium is one of the most widely studied metals with respect to hydrogen absorption. At elevated temperatures palladium nanoclusters change size due to Ostwald ripening: the larger clusters capture mobile atoms at the expense of smaller clusters [1]. As hydrogen in a metal can decrease the strength of the host metal bonding, this raises the question of how an ensemble of palladium nanoclusters will interact during and after hydrogenation. A morphological or structural change of the nanocluster ensemble may affect the hydrogenation properties as compared to a single cluster.

We investigated the effect of hydrogen exposure on a palladium cluster assembled film produced with a dual-target dual-laser vaporisation source with three different techniques: extended X-ray absorption fine structure (EXAFS), X-ray diffraction (XRD) and scanning-tunnelling microscopy (STM). These three complementary methods were used to determine the size changes of the palladium nanoclusters upon exposure to hydrogen and oxygen. The average grain size was derived both from the coordination number around palladium atoms obtained from EXAFS (Figure 23) and the width of the XRD Bragg peaks, whereas the (lateral) diameter of the nanoclusters at the sample surface was measured directly by STM. X-ray absorption data (Figure 23) collected at the DUBBLE beamline (BM26A) yielded additional parameters such as inter-atomic distances, degree of disorder and electronic information through the shift of the absorption edge; these support the observation of size changes. Upon hydrogenation, the increase in the nanocluster size measured with XRD, EXAFS, and STM is 22%, 38%, and 37%, respectively. This increase is much larger than the increase of about 8.1% in the Pd phase unit cell volume corresponding to the hydride formation. The cluster growth is due to an atomic reorganisation by three-dimensional Ostwald ripening, in which the larger clusters take up mobile atoms at the expense of smaller clusters [1]. For most materials, spontaneous Ostwald ripening is an extremely slow process at room temperature. However, the presence of a hydrogen atom in the metal reduces the binding energy, thus increasing the probability of

Fig. 23: Phase-corrected Fourier transforms of the k^3 -weighted Pd nanocluster EXAFS as a function of the atomic distance (R).

